11th International Conference
1-3 July 2013
Pisa
RASD 2013

THE EFFECT OF CUBIC DAMPING ON A BASE EXCITED ISOLATOR: AN EXPERIMENTAL STUDY FOR HARMONIC EXCITATION

Nuttarut Pananda*, Neil S. Ferguson and Timothy P. Waters

Institute of Sound and Vibration Research (ISVR)
University of Southampton
Southampton, SO17 1BJ, UK
np2g09@soton.ac.uk

Keywords: Cubic damping, Vibration isolation.

ABSTRACT

An experimental study has been conducted to validate theoretical solutions for the response of a base excited single degree-of-freedom isolation system possessing pure cubic damping. The cubic damping characteristic was implemented using an electromagnetic shaker with a simple non-linear velocity feedback control. The rig and practical implementation of the active damping are described. The base excitation was harmonic at a set of discrete frequencies with constant displacement amplitude. Consistent with theoretical predictions, the isolation performance at high excitation frequencies is shown to be worse than either the undamped or linear viscously damped isolation system with the displacement transmissibility tending to unity. This is contrary to the case of force excitation reported in the literature where cubic damping offers improved performance. The physical causes of the distinct behaviours and the consequences for isolator design are discussed.

1. INTRODUCTION

Vibration isolation is introduced to a mechanical system in order to reduce the severity of the response of the system caused by sources of vibration. The isolation system is often modelled as a single degree-of-freedom (SDOF) system. The stiffness and damping, which represent the physical isolation element, are commonly assumed to be linear and working in parallel to each other. These components are also assumed to be massless compared to the actual mass of the system. The assumption of linearity is convenient and often valid for low amplitude response.

However, in reality, the stiffness and damping components are non-linear in some aspects. Here passive non-linear damping is introduced into the isolation model. The non-linear damping in this study is characterized by a polynomial of the odd power expansion in terms of the velocity. This type of damping characteristic is said to be an anti-symmetric. The applications of the anti-symmetric non-linear damping in the force excited isolation model subject to harmonic excitation were reported to be beneficial to the system. For example, Jing et al. [1] included anti-symmetric nonlinear damping into the SDOF force excited isolation model. The powers of the velocity were 1 and 3, which is the combination of linear viscous and cubic damping. The frequency domain analysis carried out by the Volterra series expansion was verified by simulation. The results revealed that the cubic damping provides a significant re-

duction in the response at the natural frequency but has no effect on the response for the high excitation frequencies.

Peng et al. [2] studied the effect of anti-symmetric damping on the force excited isolation system for which the powers of velocity were a combination of 1, 3 and 5. The theoretical analysis and the numerical verification revealed that the presence of the non-linear terms results in a reduction of the responses around the resonance frequency and isolation region. The most recent experimental works were reported by Laalej et al. [3] and [4]. The cubic damping was incorporated for the case of force excited isolation. The experimental results showed a good agreement, the benefit of cubic damping being to reduce the transmitted force for high frequency excitation. Moreover, Tang el al. [5] introduced geometrically nonlinear damping where the viscous damping was orientated at 90° to the spring. For the case of force excitation, the response for such a system was comparable to that for the conventional system with cubic damping.

The use of cubic damping for base excited isolation has also been widely studied. For example, Shekhar et al. [6] studied a variety of isolator and absorber models subject to shock excitation. The SDOF system subject to base excitation was one of the models studied. The authors concluded that, in this case, cubic damping is detrimental to the system since the level of response increased with increasing input severity. Kovacic et al. [7] and Milovanovic et al. [8] applied the method of averaging to obtain the theoretical solution for harmonic base excitation. Only the cubic form of damping was included in the isolation model. The results showed a higher level for the displacement transmissibility tending towards unity as frequency increases. Peng et al. [9] examined both the force and base excited isolation model possessing linear plus cubic damping using the harmonic balance method. They concluded that the influence of cubic damping is dependent on the type and strength of the excitation input.

In addition, the present authors studied the effect of cubic damping in the application of an automotive vehicle suspension model [10]. The effect of cubic damping was investigated in both SDOF and 2-DOF quarter-car models in comparison to that of the SDOF force excited isolation model. It was found that cubic damping produces reduction of the force transmissibility in the isolation region. Conversely, for the case of base excitation, the cubic damping causes a high level of displacement transmissibility towards unity as the excitation frequency increased. According to the response of the SDOF base excitation, the response of the sprung mass around the wheel-hop mode for the 2-DOF model was found to be higher and broader. This behaviour was known to result from the cubic damping.

As far as the present authors are concerned, there has not been any experimental validation of the effect of cubic damping on the base excited isolation system. Thus the effect of cubic damping for the vibration isolator under harmonic excitation was investigated experimentally and is reported in this paper.

2. THEORETICAL BACKGROUND

The dynamic behaviour of a SDOF base excited isolation system possessing cubic damping has been studied. A dynamical model used in this study is shown in Figure 1. The damping component is the combination of linear viscous and cubic damping. An equation of motion for the model is given by

$$m\ddot{z} + c_1\dot{z} + c_3\left(\dot{z}\right)^3 + kz = -m\ddot{x}_0 \tag{1}$$

where z is the relative motion between the isolated mass, x, and the base excitation, x_0 and is defined by $z = x - x_0$.

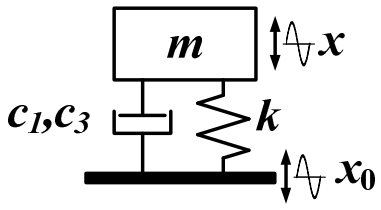

Figure 1. A single degree-of-freedom (SDOF) base excited isolation model with the combination of linear viscous c_1 and cubic damping c_3 and linear stiffness k.

The harmonic base excitation is given as $x_0 = X_0 \cos(\omega t - \phi)$ where X_0 is the amplitude of excitation, ω is the angular excitation frequency. By introducing the non-dimensional parameters, i.e. $\Omega = \dfrac{\omega}{\omega_n}$ and $\tau = \omega_n t$, equation (1) can be written in non-dimensional form with input normalisation as

$$u'' + 2\zeta_1 u' + \zeta_3 (u')^3 + u = -w_0'' \tag{2}$$

where u is the normalised relative motion given by $z = uX_0$. w_0'' is the normalised acceleration of the base given by $\ddot{x}_0 = \omega^2 w_0'' X_0$. The non-dimensional form of the cubic damping term in equation (2) is given by

$$\zeta_3 = \frac{c_3}{\sqrt{(km)^3}} (kX_0)^2 \tag{3}$$

Equation (3) indicates that the value of the non-dimensional cubic damping term varies with the amplitude of the input displacement squared. Approximate solutions for such a model were reported in the literature using a variety of methods. For example, the concept of output frequency response functions (OFRFs) was applied, see [2] and [11], or the method of averaging was applied in [7] and [8]. Here the approximate solution for equation (2) with $\zeta_1 = 0$ are obtained using the harmonic balance method and is given by

$$U^2 = \frac{1}{6} \frac{\left(108\Omega^4 B + 12\sqrt{12A^6 + 81\Omega^8 B^2}\right)^{\frac{2}{3}} - 12A^2}{B\left(108\Omega^4 B + 12\sqrt{12A^6 + 81\Omega^8 B^2}\right)^{\frac{1}{3}}} \tag{4}$$

where U is the normalised amplitude of the relative motion, $A = 1 - \Omega^2$ and $B = \dfrac{3}{4}\zeta_3 \Omega^3$. The normalised absolute motion of the isolated mass is subsequently determined from

$$W^2 = U^2 + 2U \frac{A}{\sqrt{A^2 + (BU^2)^2}} + 1 \tag{5}$$

The approximate result shown in equation (5) is plotted numerically in comparison with the experimental results later in section 5. In addition, the approximate solution obtained was analysed analytically for four excitation frequency regions. The analytical approximations are briefly shown in Table 1. These results represent the displacement amplitude ratio of an iso-

lated mass and a base excitation. Thus a term amplitude ratio is used throughout this paper. The results for the linear viscously damped system are listed for comparison with those for the cubic damping system. These analytical results will be compared and discussed with the experimental results in section 5.

Frequency region	Linear viscous damping	Cubic damping
$\Omega \ll 1$	$T^2 = 1$	$W^2 \approx 1$
$\Omega \approx 1$	$T^2 = 1 + \frac{1}{(2\zeta_1)^2}$	$W^2 \approx 1 + \left(\frac{4}{3\zeta_3}\right)^{\frac{2}{3}}$
$\Omega \approx \sqrt{2}$	$T^2 = 1$	$W^2 \approx 1$
$\Omega \gg 1$	$T^2 = \frac{(2\zeta_1)^2}{\Omega^2}$	$W^2 \approx 1 - \left(\frac{4}{3\zeta_3\Omega}\right)^{\frac{2}{3}}$

Table 1 : Approximate expressions of the amplitude ratio in four excitation frequency regions where T is the amplitude ratio for the linear viscously damped system and W is the amplitude ratio for the pure cubic damping system when $\zeta_1 = 0$.

3. EXPERIMENTAL RIG DESIGN AND SET UP

An experimental rig was designed as a simple SDOF base excitation system. The damping component was implemented using an electromagnetic shaker LDS model V101. Initially, an isolated mass was considered to be an assembly of a shaker and a mounting plate and was supported by two helical springs as shown in Figure 2 (a).

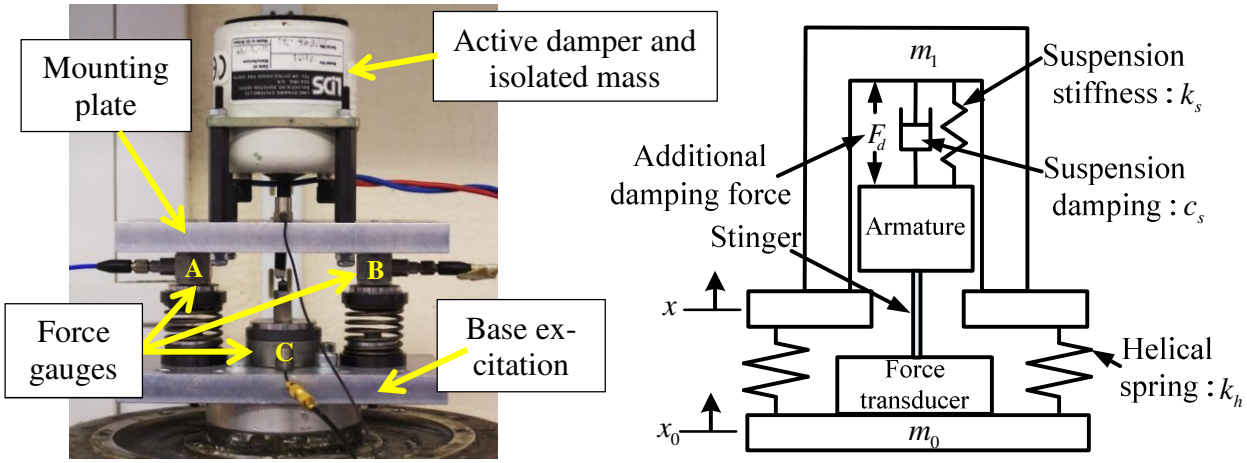

(a) (b)

Figure 2. (a) The experimental rig for a SDOF base excited isolation system and (b) dynamical representation of the experimental system.

Figure 2 (b) shows that the isolated mass is also supported by the suspension of the shaker. Thus an axial stiffness of the shaker is included into the total stiffness of the system. The approximate stiffness values of the helical spring and axial stiffness of the shaker are provided

in the specifications which are 1.00 kN/m and 3.15 kN/m respectively. Hence the total stiffness for the vertical direction is about 5.15 kN/m, and the frequency of the bounce mode could be estimated.

For the steel helical spring which is placed between two flat and parallel surfaces, internal resonances can be expected. These frequencies can be estimated by [12]

$$\omega_{nh} = n\pi\sqrt{\frac{k_h}{m_h}} \qquad n = 1, 2, 3, \ldots \tag{6}$$

where k_h is the static stiffness of a helical spring and m_h is the mass of the helical spring. These parameters are respectively given by

$$k_h = \frac{Gd^4}{8N_L D^3} \tag{7}$$

$$m_h = \frac{\pi^2 \rho N D d^2}{4} \tag{8}$$

where G is the shear modulus, d is the wire diameter, D is the mean diameter of the coil, N_L and N are the number of loaded coils and complete coils respectively and ρ is the density of the spring material. The predicted frequency for the first internal resonance is 204 Hz. Thus the most suitable frequency range for the measurement should be lower than this frequency.

In addition, the lowest frequency for the measurement is limited by the ability of the equipment, e.g. accelerometers and power amplifiers. Some equipment cannot perform very well for very low frequency. The low frequency limit was initially desired to be 5 Hz. Then the bounce frequency was chosen to be about 10 Hz. Thus a total mass of 1.3 kilograms for the isolated mass was required.

Moreover, as the isolated mass was being supported by the two helical springs, there should exist a pitch frequency. The frequency of the pitch mode is dependent upon the distance between the centres of the two helical springs. Thus the distance between the centres of two helical springs was designed to produce a corresponding pitching frequency lower than 5 Hz. The mounting plate was then manufactured and the complete experimental rig is as shown in Figure 2 (a). Figure 2 (b) illustrates how the isolated mass is suspended.

The frequency response of the rig without any additional active damping appeared to resemble well the SDOF system in the frequency range of 7-100 Hz, as shown in Figure 3 with no noticeable contribution due to the pitching mode. The appearance of small peak around 20 Hz is likely to be an additional rigid body mode, possibly a rolling mode. The symmetric design of the experimental rig produced, as far as possible, uncoupled rigid body modes for the mounting plate. The occurrence of the resonance peaks around 200 Hz were identifiable as the internal resonances of the isolator springs.

The bounce mode natural frequency and passive damping ratio were determined from the measured transfer functions. These parameters were calculated using two different tools, i.e. the circle fit method [13] and the MATLAB function ‘invfreqs’ [14]. The calculated bounce natural frequency was about 11 Hz and the corresponding linear viscous damping ratio was about 0.04. The plot shown in Figure 3 includes the mathematical estimation of the linear system which fits the experimental data reasonably well.

A mathematical estimation of the linear system shown in Figure 3 was initially obtained using the model illustrated in Figure 1. The equation of motion for such a model can be represented by a simple SDOF vibration isolation system. To incorporate the dynamics and the

mass of the base, for the experimental rig shown in Figure 2 (b), the system is represented using a two degree-of-freedom (2DOF) system. The equations of motion are given by

$$m_0\ddot{x}_0 + c_s\left(\dot{x}_0 - \dot{x}_1\right) + \left(k_h + k_s\right)\left(x_0 - x_1\right) + f_d = f_e \tag{9}$$

$$m_1\ddot{x}_1 + c_s\left(\dot{x}_1 - \dot{x}_0\right) + \left(k_h + k_s\right)\left(x_1 - x_0\right) - f_d = 0 \tag{10}$$

where m_0 is the mass of the base excitation, m_1 is the isolated mass, c_s is the passive damping coefficient for the shaker suspension, k_s is the stiffness of the shaker suspension, k_h is the total stiffness of the helical springs, f_d is the damping force to be produced or additional damping force and f_e is an external force applied to the base.

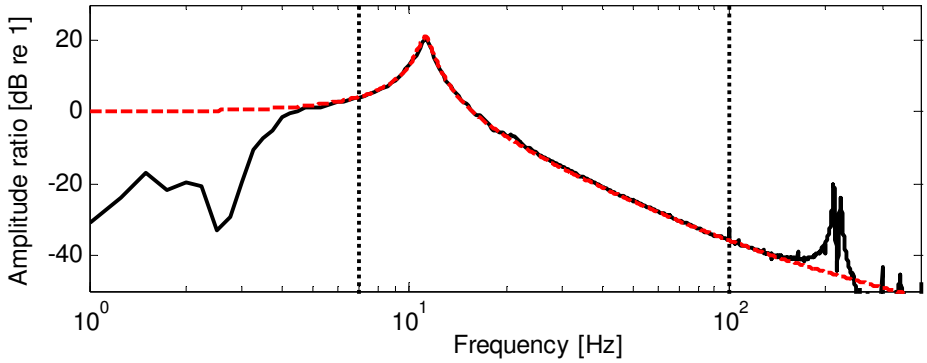

Figure 3. Displacement amplitude ratio of the SDOF base excited isolation system subject to white noise (0–20 kHz) with no damping control; (—) experimental results, (- - -) a fit to the data using a SDOF linearly damped model

In order to simulate an additional damping characteristic such as linear damping or cubic damping, a feedback control unit was required. The control process was implemented using velocity feedback control. The control diagram is shown in Figure 4. The velocity signals of the base excitation and isolated mass were obtained from the charge amplifiers which integrated the acquired acceleration signals. The relative velocity was calculated within the control unit. The control unit has the ability to process an arbitrary damping configuration, in this instance linear and cubic damping configurations were considered. The data processing unit sampled the signal at a sample rate of 6 kHz. As a result, with the highest excitation frequency of 100 Hz, there was no effect from the delay of the feedback signals.

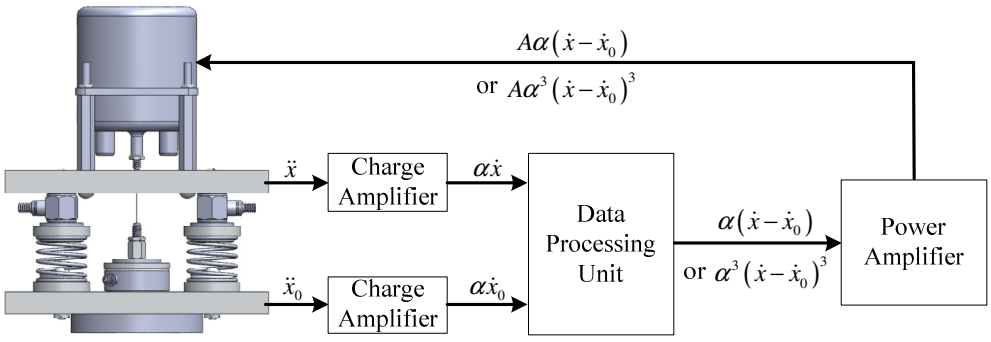

Figure 4. Block diagram of the feedback loop; $\ddot{x}$ and $\ddot{x}_0$ are acceleration, $\dot{x}$ and $\dot{x}_0$ are velocity of the isolated mass and base input, α and A are the gains from the charge amplifier and shaker amplifier respectively

4. EXPERIMENTAL CONDITIONS

As mentioned in the previous section, the data processing unit is able to produce an arbitrary damping characteristic. The additional linear damping and cubic damping were respectively produced as in this case study. The excitation for both cases was considered initially as a set of discrete frequencies ranging from 7-100 Hz with constant displacement amplitude. Two amplitude levels were chosen for the applied displacement excitation, i.e. 0.04 mm and 0.06 mm.

The maximum excitation amplitude was calculated referring to the response of the passive system as shown in Figure 3. The level of amplitude ratio around resonance is about 20 dB hence the amplitude of the isolated mass would be about 10 times higher than the amplitude of the input. The peak to peak displacement of the active damper is limited to 2.5 mm. To avoid damage and unwanted force from the end-stop, the peak to peak amplitude of relative displacement was considered to be less than 50% of the limitation. Thus the peak to peak relative displacement should not exceed 1.25 mm. Therefore an input amplitude of 0.06 mm was chosen. This level of the input amplitude resulted in a peak to peak relative displacement of around 1.24 mm. However, practically, a constant input amplitude of 0.06 mm for the excitation frequencies higher than 80 Hz could not be achieved. This was limited by the base shaker excitation. Thus the maximum excitation frequency was set to 80 Hz.

The measurements for both linear and cubic damping cases were done in two separate scenarios, namely when (a) the input base amplitude was specified and controlled and when (b) the damping level was specified and controlled. For the first scenario, for a given fixed value of damping the amplitude of the base displacement was chosen to be at two different levels. Case (b) was done by exciting at one constant level for the base displacement input and selecting the level of the damping. In order to obtain reasonable results, the peak values of the amplitude ratio (transmissibility) around resonance were chosen to be approximately 15 dB for lower damping and 10 dB for higher damping. By doing this the effect of cubic damping can be distinguished from the case of the linearly damped system for the given peak levels.

5. IMPLEMENTATION OF ADDITIONAL DAMPING AND RESULTS

The results obtained from the measurements are described in the format of the displacement amplitude ratio. This quantity represents the ratio of the displacement amplitude between the isolated mass and base excitation. The amplitude ratio for the experimental results can be constructed using either root mean square (RMS) values or the Fourier coefficients at the excitation frequency. Both quantities can be calculated from the acquired time histories. However, the reader might note that, in this paper, only the amplitude ratio constructed using Fourier coefficients at the excitation frequencies are used. The plots of these two quantities were very similar in the frequency range of interest and the comparison between these plots is omitted for brevity.

5.1 Linear damping implementation

The response for the system without an additional or active damping is described in Section 3. It is seen that the system has an apparent passive damping which is equivalent to a linear viscous damping ratio of 0.04. In this section, the responses when the active linear damping was implemented are shown. The active linear damping was built up using velocity feedback according to the control schematic shown in Figure 4. The amplitude of the gain $A\alpha$ represents the value of damping coefficient. Adjusting the gain $A\alpha$ yields the change of the amplitude ratio. In this experiment, the level of the amplitude ratio around resonance frequency was fixed at two levels as mentioned in Section 4.

Theoretically, the change in amplitude of the input does not affect the amplitude ratio of the linear system as long as the value of damping is constant. The level of the amplitude ratio at resonance for the linearly damped system depends only upon the value of the damping ratio. Figure 5 (a) shows the plots of the amplitude spectra for the fixed higher value of

damping but two different excitation levels, i.e. 0.04 mm and 0.06 mm. Figure 5 (b) shows the amplitude ratios obtained from both excitation levels in comparison with the theoretical estimation. These plots clearly show that, for the linearly damped system, the amplitude of input excitation does not have an influence on the amplitude ratio.

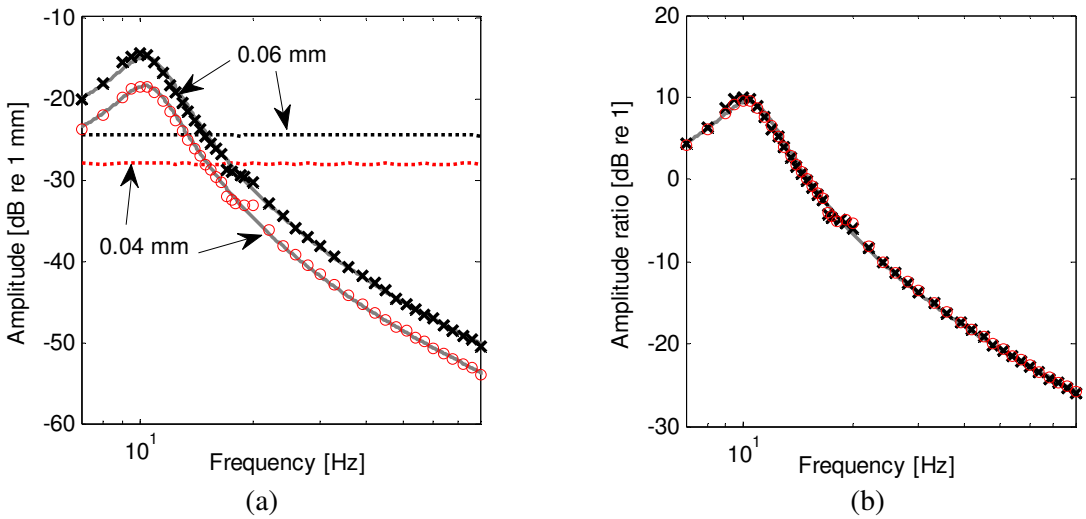

Figure 5. Plots of the measured base and isolated mass displacement amplitudes and the transmissibility (amplitude ratio) for linearly damped isolation at two excitation amplitudes and discrete frequency excitation. (a) Amplitude spectra and (b) Displacement amplitude ratio. O represents the responses for the 0.04 mm excitation, × response for the 0.06 mm excitation, (·····) base displacement excitation, and (——) theoretical result with $\zeta_1 \approx 0.18$.

For the second scenario, the amplitude of excitation was kept constant at 0.04 mm but the value of damping was adjusted for two different values corresponding to the peaks values of the amplitude ratio. The amplitude ratios are plotted in comparison to the theoretical estimate as shown in Figure 6. These are consistent with the theoretical results listed in Table 1 which show that increasing the value of damping reduces the response around resonance but raises the level of the amplitude ratio in the isolation region. This is the classic characteristic of linear viscous damping.

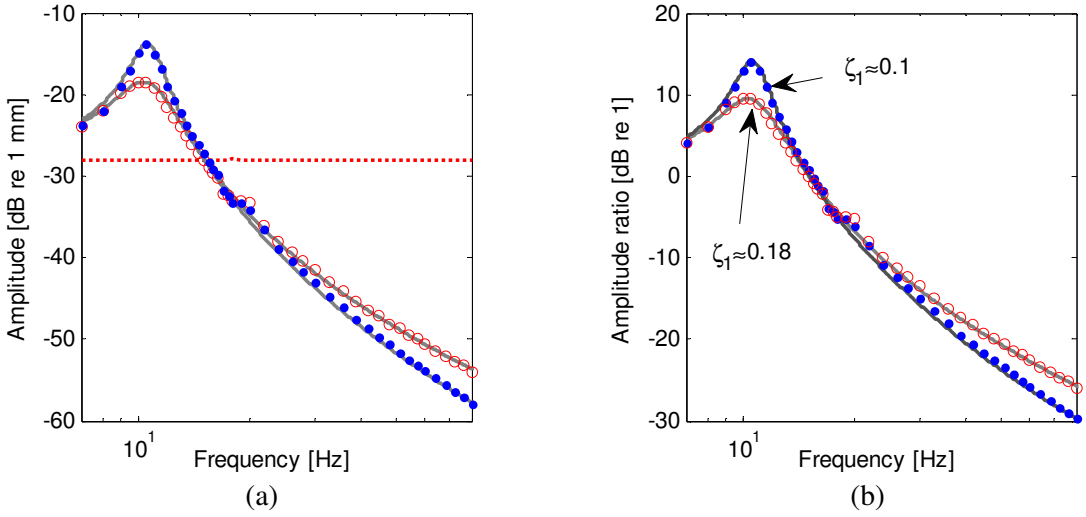

Figure 6. Plots of the measured base and isolated mass displacement amplitudes and the transmissibility (amplitude ratio) for linearly damped isolation at one excitation amplitude (0.04 mm) for two levels of linear damping and discrete frequency excitation. (a) Amplitude spectra and (b) Displacement amplitude ratio. • represent response for lower damping, O response for the higher damping, (·····) base displacement excitation and (——) theoretical results.

5.2 Cubic damping implementation

The cubic damping was set up by raising the relative velocity to the power of three. The cubic damping coefficient was determined by the amplifier gain. The cubic damping was added to the system as an additional damping to the linear passive damping of the system. The measurements were done in the same way as that for the case of the linearly damped configurations. The values of the cubic damping terms were determined by referring to the levels of the response around resonance, i.e. around 15 dB re 1 and 10 dB re 1 for lower and higher damping respectively.

The experimental investigation into the effect of cubic damping began by increasing the displacement amplitude of the base excitation. The displacement amplitude was increased to be 0.06 mm, whilst the lower value of cubic damping coefficient was applied. The amplitude spectra for the two different base displacement input excitation levels are shown in Figure 7 (a). Apparently the amplitude spectrum of the response for the higher excitation amplitude is higher. This appeared similar to that for the case of linearly damped system in which the higher excitation amplitude results in a higher level of response.

However, considering the plot of the amplitude ratios as shown in Figure 7 (b), it is seen that these ratios are different. The amplitude ratio for the higher excitation amplitude appeared to be lower in the region of resonance frequency and higher for the high excitation frequencies above resonance. It can be concluded that increasing excitation amplitude results in a higher value of effective cubic damping. This is consistent with the theoretical expression given in equation (3) which shows that the non-dimensional cubic damping is proportional to the excitation amplitude squared. As a result that the effective value of cubic damping is defined by the excitation amplitude, the response of the system is also dependent on the excitation amplitude.

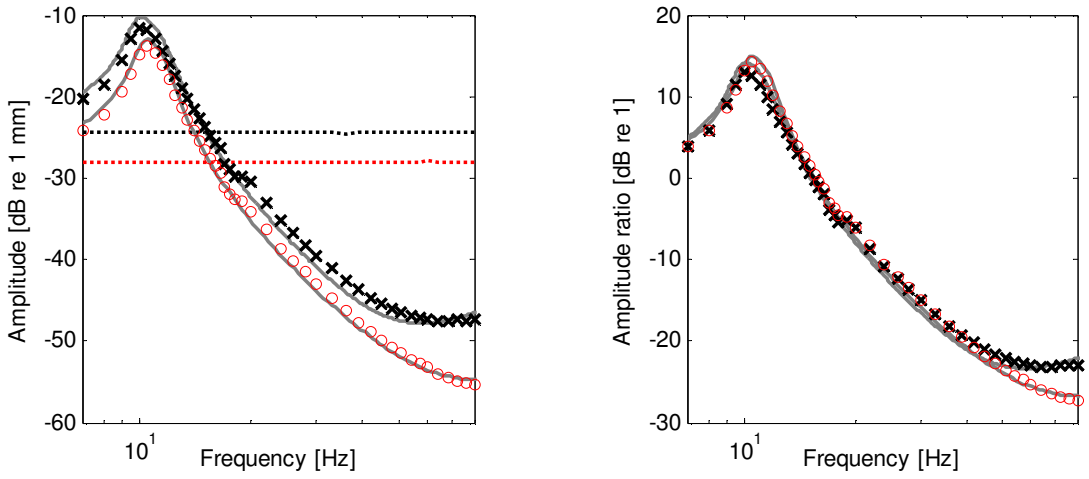

Figure 7. Plots of the measured base and isolated mass displacement amplitudes and the transmissibility (amplitude ratio) for the cubic damped isolation at two excitation amplitudes (0.04 and 0.06 mm) for one level of cubic damping and discrete frequency excitation. (a) Amplitude spectra of base excitation and isolated mass and (b) Displacement amplitude ratio. O represent response for the 0.04 mm, × response for the 0.06 mm excitations, (·····) base displacement excitation and (——) theoretical responses.

The amplitude spectra of responses for the system with two different values of cubic damping coefficient subject to constant input amplitude of 0.04 mm are plotted in Figure 8 (a). These results fit fairly well the approximate solution obtained using equations (4) and (5). Figure 8 (b) shows the plots of amplitude ratio in comparison with the linearly damped responses. These plots show that for a similar level of the response around resonance, the

responses for the systems with cubic damping appeared to be higher than those for the linearly damped system in the isolation region.

This is also shown by the approximate expressions listed in Table 1 as for $\Omega \gg 1$. For higher excitation frequencies the displacement amplitude ratio tends towards unity. The value of the cubic damping controls the rate at which the response increases, i.e. a higher value of the cubic damping coefficient causes a more rapid increase towards a displacement ratio of unity.

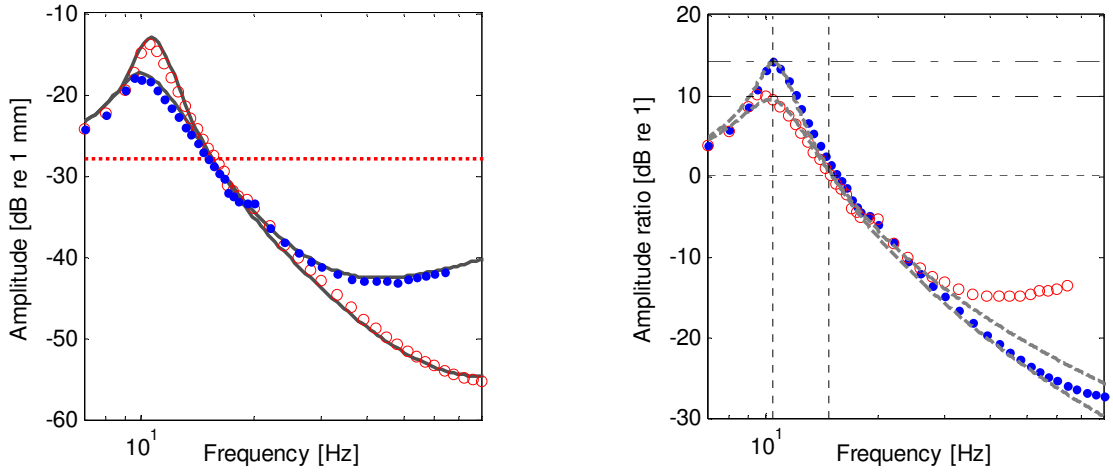

(a) (b)

Figure 8. Plots of the measured base and isolated mass displacement amplitudes and the transmissibility (amplitude ratio) for the cubic damped isolation at one excitation amplitude (0.04 mm) for two levels of cubic damping and discrete frequency excitation. (a) Amplitude spectra and (b) Displacement amplitude ratio. O responses for lower level cubic damping, • responses for higher cubic damping, (·····) base excitation, (——) theoretical nonlinear results, (– – –) theoretical linear results for $\zeta_1 \approx 0.1$ and $\zeta_1 \approx 0.18$, and (–·–) approximate responses for $\omega \approx \omega_n$ and $\omega \approx \sqrt{2}\omega_n$ given by Table 1.

5.3 The theoretical and measured forces

In order to compare and validate the model for the linear and nonlinear damping cases, which were produced by the secondary actuator and incorporated its dynamics, the study considered the measured forces produced by the helical isolation springs and also the force produced by the secondary actuator.

Apart from the theoretical approximations obtained using the harmonic balance method, numerical integration was also applied to obtain numerical results. Equations (9) and (10) were integrated numerically using ODE45 in MATLAB. The results obtained can be used to determine the theoretical forces. Referring to the model illustrated in Figure 2 (b), the forces can be considered as follows;

- The sum of the restoring forces resulting from the helical springs is given by

$$f_h = k_h \left(x_1 - x_0 \right) \tag{11}$$

- The sum of the forces (internal passive actuator restoring forces and the active damping force) being produced by an active damper is given by

$$f_s = c_s \left(\dot{x}_1 - \dot{x}_0 \right) + k_s \left(x_1 - x_0 \right) + f_d \tag{12}$$

where f_d is the additional damping force which can be considered as linear damping, i.e. $f_d = c_1 \left(\dot{x}_1 - \dot{x}_0 \right)$, or cubic damping, i.e. $f_d = c_3 \left(\dot{x}_1 - \dot{x}_0 \right)^3$. In addition to the expressions given

in equations (11) and (12), the inertia force must be taken into account. This is because the mass of equipment involved is not negligible with respect to the isolated mass [15], i.e. the mass of the force transducers and of the spring washers.

Figure 2 (a) shows the three force transducers that were used to acquire the actual forces. The forces acquired using the force transducers A and B can be referred to as the restoring forces which were the result of the helical springs. The sum of these forces is equivalent to f_h given in equation (11). Figure 9 shows the comparison of the restoring forces directly acquired from transducers A and B and the calculated forces given in equation (11). Note that, the calculated force includes the force of inertia resulting from the mass of force transducers and spring washers. This shows consistency with the measured results.

The force transducer C in the middle measured the force produced from the secondary actuator which produces the cubic damping. The force acquired is equivalent to f_s given in equation (12). The mass of the force transducer is not negligible with respect to the mass of the system. So inertia forces must be considered. This means that the forces acquired by transducer C include the inertia force resulting from the mass of transducer C. The theoretical and measured forces are plotted as a function of frequency as shown in Figure 10. Note that, the plots of forces shown in Figures 9 and 10 correspond to the case of higher value of damping which the amplitude ratio was controlled to be about 10 dB.

Figures 10 (a) and (b) show the forces acquired by transducer C for the cases of linear and cubic damping respectively. One can see that the level of force around the resonance frequency is about the same for both cases. This is a consequence of keeping the level of the amplitude ratio around resonance to be the same. The difference in the force level is noticeable for excitation frequencies above 30 Hz. At this frequency, the amplitude ratio for the system with higher cubic damping starts to increase and diverge from the linear response. This can be ascribed to the higher level of the damping force.

The level of damping force is dependent upon the relative velocity across the damper. For the SDOF linear base excited isolation system, the relative velocity across the damper is proportional to the excitation frequency. Hence at higher excitation frequencies this results in a higher relative velocity. So the damping force is higher as consequent result. It is evident in Figure 10 that the force for the system with cubic damping is much higher than for the linear damping for the excitation frequencies high above resonance. Eventually, the damping component can be considered as a rigid-link.

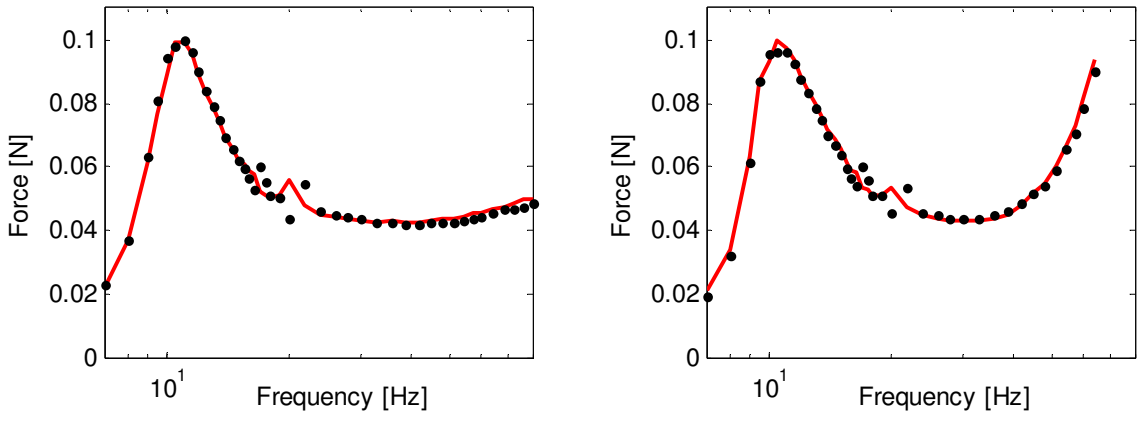

Figure 9. The total measured helical springs' isolation restoring force for isolation with an approximate level for the peak amplitude ratio of 10 dB for (a) linear damping and (b) cubic damping with • representing the measured forces and (—) represent the calculated forces using the measured relative velocity, which is integrated and substituted into equation (11)

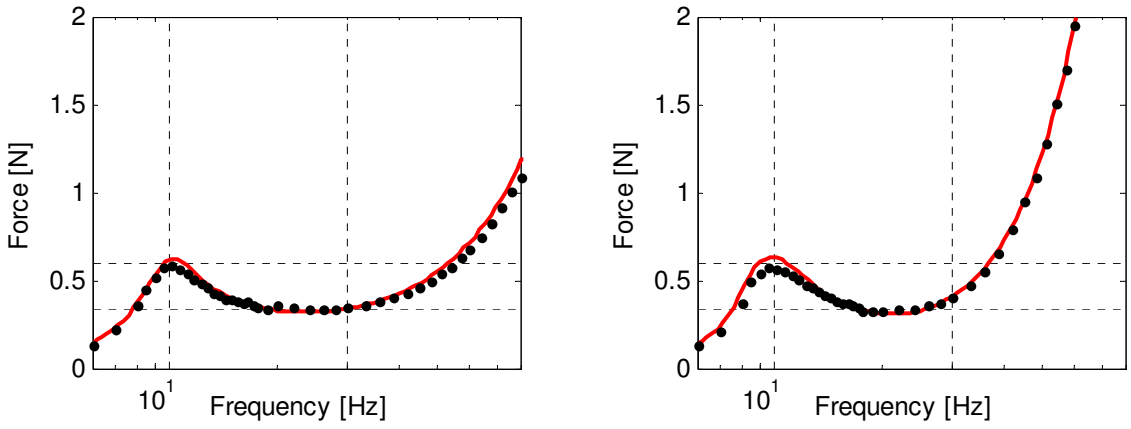

Figure 10. The measured secondary actuator force for isolation with an approximate level for the peak amplitude ratio of 10 dB for (a) linear damping and (b) cubic damping with • representing the measured forces and (—) represent the theoretical force f_s evaluated using equation (12) and the measured relative velocity.

6. CONCLUSIONS

An experimental study on a SDOF base excited isolation system was conducted in order to investigate and validate the effect of cubic damping, which has been reported theoretically in the literature. A set of discrete frequency harmonic base excitation was applied. The amplitude of the base excitation was controlled to produce a constant displacement amplitude. Two damping configurations, linear and cubic damping, were implemented using an active damper with velocity feedback. The investigation in the effect of cubic damping was done by comparing the responses to that for the linear damping configuration. The responses around resonance for both scenarios were controlled to have similar levels in order to distinguish the effect of cubic damping from the linear damping at high excitation frequencies. The experimental results appeared to be in agreement with the theoretical results. The cubic damping produces large damping forces for the excitation frequencies high above resonance compared to that for the linear case. This characteristic causes a high amplitude in the isolated mass. One might thus conclude that using cubic damping in the SDOF base excited isolation model subject to discrete harmonic excitation, with constant displacement amplitude is not beneficial.

REFERENCES

[1] X. Jing and Z. Lang, Frequency domain analysis of a dimensionless cubic nonlinear damping system subject to harmonic input, *Nonlinear Dynamics,* 58(3), pp. 469-485, 2009.

[2] Z. K. Peng, Z. Q. Lang, X. J. Jing, S. A. Billings, G. R. Tomlinson and L. Z. Guo, The transmissibility of vibration isolators with a nonlinear antisymmetric damping characteristic, *Journal of Vibration and Acoustics,* 132(1), pp. 1-7, 2010.

[3] H. Laalej, Z. Q. Lang, S. Daley, I. Zazas, S. A. Billings and G. R. Tomlinson, Application of non-linear damping to vibration isolation: an experimental study, *Nonlinear Dynamics,* 69(1-2), pp. 409-421, 2012.

[4] H. Laalej, Z. Q. Lang, B. Sapinski and P. Martynowicz, MR damper based implementation of nonlinear damping for a pitch plane suspension system, *Smart Materials and Structures,* 21(4), pp. 1-14, 2012.

[5] B. Tang and M. J. Brennan, A comparison of two nonlinear damping mechanisms in a vibration isolator, *Journal of Sound and Vibration,* 332(3), pp. 510-520, 2013.

[6] C. N. Shekhar, H. Hatwal and A. K. Mallik, Performance of non-linear isolators and absorbers to shock excitations, *Journal of Sound and Vibration,* 227(2), pp. 293-307, 1999.

[7] I. Kovačić, Z. Milovanović and M. J. Brennan, On the relative and absolute transmissibility of a vibration isolation system subjected to base exctation, *FACTA UNIVERSITATIS Series: Working and Living Environmental Protection,* 5(1), pp. 39 - 48, 2008.

[8] Z. Milovanovic, I. Kovacic and M. J. Brennan, On the displacement transmissibility of a base excited viscously damped nonlinear vibration isolator, *Journal of Vibration and Acoustics,* 131, pp. 1-7, 2009.

[9] Z. K. Peng, G. Meng, Z. Q. Lang, W. M. Zhang and F. L. Chu, Study of the effects of cubic nonlinear damping on vibration isolations using Harmonic Balance Method, *International Journal of Non-Linear Mechanics,* 47(10), pp. 1073-1080, 2012.

[10] N. Panananda, N. S. Ferguson and T. P. Waters, The effect of cubic damping in an automotive vehicle, *Proceeding of the International Symposium on the Computational Modelling and Analysis of Vehicle Body Noise and Vibration*, *University of Sussex, Brighton, UK*, 2012.

[11] Z. Q. Lang, X. J. Jing, S. A. Billings, G. R. Tomlinson and Z. K. Peng, Theoretical study of the effects of nonlinear viscous damping on vibration isolation of sdof systems, *Journal of Sound and Vibration,* 323(1–2), pp. 352-365, 2009.

[12] B. Yan, M. J. Brennan, S. J. Elliott and N. S. Ferguson, Characteristics of distributed parameter isolators, *Journal of Sound and Vibration,* 320(3), pp. 516-526, 2009.

[13] D. J. Ewins, *Modal testing : theory, practice and application*, 2nd ed. Hertfordshire, England: Research studies press Ltd., 2000.

[14] P. S. R. Dinz, E. A. B. d. Silva and S. L. Netto, *Digital signal processing : system analysis and design*. Cambridge, UK: Cambridge University Press, 2002.

[15] T. Olbrechts, P. Sas and D. Vandepitte, FRF Measurements Errors Caused by the Use of Inertia Mass Shakers *Proceeding of the 15th International Modal Analysis Conference Orlando, USA.*, pp. 188-194, 1997.